Triaxiality and shape coexistence in germanium isotopes

Lu Guo,[1] J. A. Maruhn,[1] and P.-G. Reinhard[2]
[1]*Institut für Theoretische Physik, J. W. Goethe-Universität, D-60438 Frankfurt, Germany*
[2]*Institut für Theoretische Physik II, Universität Erlangen-Nürnberg, Staudtstrasse 7, D-91058 Erlangen, Germany*
(Received 15 January 2007; published 19 September 2007)

The ground-state deformations of the Ge isotopes are investigated in the framework of Gogny-Hartree-Fock-Bogoliubov (HFB) and Skyrme Hartree-Fock plus pairing in the BCS approximation. Five different Skyrme parametrizations are used to explore the influence of different effective masses and spin-orbit models. There is generally good agreement for binding energies and deformations (total quadrupole moment and triaxiality) with experimental data where available (i.e., in the valley of stability). All calculations agree in predicting a strong tendency for triaxial shapes in the Ge isotopes with only a few exceptions owing to neutron (sub)shell closures. The frequent occurrence of energetically very close shape isomers indicates that the underlying deformation energy landscape is very soft. The general triaxial softness of the Ge isotopes is demonstrated in the fully triaxial potential energy surface. The differences between the forces play an increasing role with increasing neutron number. This concerns particularly the influence of the spin-orbit model, which has a visible effect on the trend of binding energies toward the drip line. Different effective mass plays an important role in predicting the quadrupole and triaxial deformations. The pairing strength only weakly affects binding energies and total quadrupole deformations, but it considerably influences triaxiality.

DOI: 10.1103/PhysRevC.76.034317 PACS number(s): 21.60.Jz, 21.10.Dr, 21.30.Fe, 27.50.+e

I. INTRODUCTION

In recent years, the development of radioactive nuclear beams and new γ-ray detector arrays, together with the powerful ancillary detectors for light ions, has allowed the experimental studies of nuclei close to the proton and neutron drip lines [1–3], making theoretical studies of the ground-state properties of these nuclei important. These nuclei may reveal interesting phenomena of nuclear structure physics and provide a testing ground for theoretical models, which should explain the systematics of various properties over long chains of isotopes.

Atomic nuclei exhibit a variety of shapes, varying from spherical to quadrupole and higher order multipole deformations. The possible shape that the nucleus may adopt results from a delicate balance between collective and single-particle energies and their dependence on deformation. Nuclear triaxiality, associated with the breaking of axial symmetry of the quadrupole deformation, brings up many interesting collective motions (e.g., wobbling motion and chiral and γ bands). Recent measurements of the quadrupole moments and $B(E2)$ transition probabilities from Coulomb excitation experiments [4,5] give more direct indications of nuclear triaxiality.

Various theoretical methods, including the shell model [6,7] and self-consistent mean-field models [8,9], as well as the interacting boson model [10] have been employed to predict nuclear exotic shapes. Many authors [11–13] discussed nuclear shape extensively, but imposed axial and reflection symmetries to alleviate the complex numerical problems. In axially symmetric calculations, both prolate and oblate minima with energies very close to each other can coexist in the nuclear deformation energy curve as a function of quadrupole deformation. In such cases, one cannot definitely conclude which shape is the ground-state configuration and whether there is a real shape coexistence or if there is yet another type of deformation, such as γ-instability with a valley linking the prolate and oblate shapes through the triaxial region. A study of the Zn and Ge isotopes within the relativistic mean-field theory [14] indicates that the restrictions imposed by the assumption of axial symmetry may be too severe and a triaxial calculation is necessary.

The motivation for the present work is to study the triaxiality and shape transitions in a number of Ge isotopes from the proton to the neutron drip line. These isotopes are the best candidates for examining the degree to which nuclear ground states can adopt triaxial deformation, and there are several indications from theoretical studies already for a potentially rich variation in deformation. For example, recent Hartree-Fock-Bogoliubov (HFB) calculation predicted that the nucleus ^{64}Ge is extremely soft toward triaxial deformation [15]. Triaxial Routhian surface calculations for ^{64}Ge predicted a well-deformed minimum at $\beta_2 = 0.3$ and $\gamma \approx 15^\circ$ [16]. Calculations using the IBM-3 approach [10] described ^{66}Ge and ^{68}Ge as vibrational nuclei, and an oblate shape was predicted for the ground-state band of ^{68}Ge by excited VAMPIR calculations [17]. Thus, this region should provide an excellent opportunity to test nuclear structure models. Moreover, the study of various isotope chains with different theoretical models allows the possibility to distinguish what is general from what is particular in the behavior of these nuclei.

The three most widely used self-consistent mean-field models are the Skyrme energy functional, the Gogny force, and a relativistic mean-field Lagrangian; for a recent review see Ref. [18]. In the present work two mean-field methods are employed to study the nuclear triaxiality. One is the Skyrme energy density functional plus BCS pairing (see, e.g., Ref. [19]). In this case it is to be noted that several parametrizations exist for the Skyrme functional, among which we will choose five different ones to cover a sufficient variety

of open options. The other method is the HFB theory with the Gogny interaction [20–22]. The finite-range Gogny force is designed to provide a simultaneous description of both the particle-hole (HF) and the particle-particle (pairing) channels of the mean field.

The paper is organized as follows: Section II gives a brief outline of the two theoretical models, Skyrme HF plus BCS and Gogny HFB. In Sec. III, triaxial features of the Ge isotopic chain are presented within both models. The Skyrme HF-BCS calculations predict shape isomers and γ-softness in many Ge isotopes. The effects of the spin-orbit interaction, the effective mass, and the pairing strength on the systematic properties of the Ge isotopic chain are discussed with various Skyrme forces and different pairing strengths. Our calculated ground-state properties are compared with the available experiments. Section IV is devoted to a summary.

II. THEORETICAL MODELS

A. Skyrme Hartree-Fock plus BCS

The zero-range and density-dependent Skyrme force has been widely applied to self-consistent nuclear structure calculations owing to its numerical simplicity. Various parametrizations of the Skyrme force are available, many of which provide an excellent description of basic nuclear bulk properties (binding energies, radii, etc.), but differ in other aspects (e.g., excitations, fission barriers, or neutron matter properties [23]). For this work we have chosen five typical parametrizations that differ with respect to effective mass and spin-orbit terms and with respect to the bias in the fit. The force SkM* is meanwhile an established standard, one of the first forces that managed to cover several observables with quantitative success [24]. The force SkT6 stems from a systematic survey of varied parametrizations at the level of quality in these years (see SkM*) and it is a choice having an effective nucleon mass around unity [25]. The force SkP was originally developed to compute the pairing matrix elements from the same Skyrme force as used for the mean field [26]. We take it here as an alternative for a force with unit effective mass and employ the same type of pairing force as for the other parametrizations. The force SLy6 is a recent fit including more data with emphasis on isotopic trends, neutron-rich nuclei, and neutron matter [27]. It has rather low effective mass. The force SkI3 is also a recent fit having low effective mass [28]. It employs an extended spin-orbit force, which was built in analogy to relativistic models [29]. Its fit also includes the nuclear charge form factor, which, in turn, provides a more realistic (i.e., softer) surface thickness. The effective masses for the five Skyrme parametrizations are given in column two of Table I.

The Skyrme energy functional consists of kinetic energy, Skyrme interaction energy, Coulomb energy including exchange in Slater approximation, pairing energy, and a correction for the spurious center-of-mass motion. All terms besides the center-of-mass energy can be expressed in terms of local distributions, namely density, kinetic energy density, spin-orbit current, and pair density. The pairing correlations are treated in the BCS approximation by using a delta pairing force [30,31], $V_{\rm pair}(\vec{r},\vec{r}') = V_q\delta(\vec{r}-\vec{r}')$. The pairing strength V_p for protons and V_n for neutrons depend on the mean-field parametrization. For each parametrization they are separately fitted to the pairing gaps in the selected isotopic and isotonic chains. The pairing strengths for the different Skyrme parametrizations are taken from Ref. [32] and listed in Table I. Note that they vary dramatically with the force. They depend on the actual shell structure, in particular on the effective mass. The variation of the energy functional with respect to the single-particle wave functions yields the mean-field equations and variation with respect to the occupation amplitudes gives the associated pairing equations.

TABLE I. The isoscalar effective mass m^*/m in infinite nuclear matter and the pairing strengths V_p for protons and V_n for neutrons for the Skyrme interactions used in the calculations.

Force	m^*/m	V_p (Mev fm^3)	V_n (Mev fm^3)
SkT6	1.00	−202.526	−204.977
SkP	1.00	−252.619	−236.237
SkM*	0.79	−279.082	−258.962
SLy6	0.69	−298.760	−288.523
SkI3	0.57	−335.432	−331.600

The coupled HF-BCS equations are solved on a grid in coordinate space with Fourier representation of the derivatives. No symmetry restriction has been imposed in the calculation. The stationary states are found with the damped gradient iteration method [33]. As the most sensitive criterion for convergence we take the variance of the mean-field Hamiltonian, which is required to become smaller than 10^{-4} MeV. Experience shows that this is a sufficient safeguard against being deceived by pseudo-convergence (an iteration being stuck at a certain energy value for very long times). We start the iteration from various initial states to explore the landscape of isomers that are stable stationary minima besides the ground state. Deformation and energy of the isomers help to indicate the softness of the deformation energy landscape. Note, however, that the search for isomers is only exploratory. We do not aim at unraveling the complete landscape of isomers. We rather consider the isomers that we happen to find as indicators for the softness of the underlying deformation energy landscape.

B. Gogny Hartree-Fock-Bogoliubov

We use the finite-range Gogny force with parametrization D1S [34,35]. It consists of a finite-range part with Gaussian shape containing the four relevant spin-isospin exchanges (Wigner, Majorana, Heisenberg, and Bartlett), a density-dependent zero-range term, a zero-range spin-orbit force, and the Coulomb force. Exchange field is treated exactly in all terms.

We have taken into account all the contributions to HF and pairing fields arising from the Gogny and Coulomb interactions as well as the two-body correction of the kinetic energy in the self-consistent procedure. The finite-range Gogny force allows us to derive the HF Hamiltonian and the pairing field simultaneously from one and the same Hamiltonian. The practical treatment is, of course, much more

cumbersome. To save CPU time in the numerical calculations, the $\hat{P}e^{-i\pi\hat{J}_z}$ (z-simplex) and $\hat{P}e^{-i\pi\hat{J}_y}\hat{\tau}$ ($\hat{S}_y^T$) symmetries are imposed [36,37], where $\hat{P}$ is the parity operator, $e^{-i\pi\hat{J}_i}$ the rotation operator around the i-axis with an angle π, and $\hat{\tau}$ the time reversal operator. Owing to the z-simplex and $\hat{S}_y^T$ symmetries, a mass asymmetry of the nucleus is allowed only along the x-axis.

The HFB equation has been solved in a three-dimensional harmonic oscillator basis [22,38,39]. The triaxial oscillator parameters of the Hermite polynomials were optimized for each nucleus to obtain the largest ground-state binding energy. In our calculations of the Ge isotopes, the optimization was done with an expansion of single-particle wave functions up to a principal quantum number $N_0 = 8$ in the oscillator basis. This basis size together with the optimized basis parameters provides a very good description, comparable to the calculation with 12 shells in the fixed basis [22]. No isomeric states could be calculated, however, because the optimization of the basis produces convergence only into the ground state.

III. TRIAXIALITY AND SHAPE COEXISTENCE

We discuss the properties of ground states and coexistent isomeric states for the Ge isotopes from the proton-rich isotope with neutron number $N = 26$ to neutron-rich nuclei until close to the neutron drip-line at $N = 76$.

Figure 1 shows the energies of ground states (filled symbols) and isomers (open symbols). The energies as such would have a huge variation and lead to a rather meaningless plot, so we show relative energies, in the upper panel relative to experiment and in the lower panel relative to the results from a macroscopic-microscopic model, the finite-range liquid-drop model (FRLDM) with results taken from Ref. [40]. In the range of experimentally accessible isotopes, there is a clear sorting of energies with forces, with Gogny predicting underestimated binding throughout. The older Skyrme forces (SkM*, SkT6, and SkP) tend to overbinding. The typical deviation from experiment is smallest for SLy6 and SkI3, which is no surprise because these two forces are the most recent developments in our sample. The exotic regime (i.e., the wings of the distributions) shows a much wider span of energy predictions, as is expected since the uncertainty in extrapolations grows when going farther away from the regime of stable nuclei for which the forces were adjusted. Even the ordering of energies with forces is interchanged owing to different isovector properties in the different parametrizations.

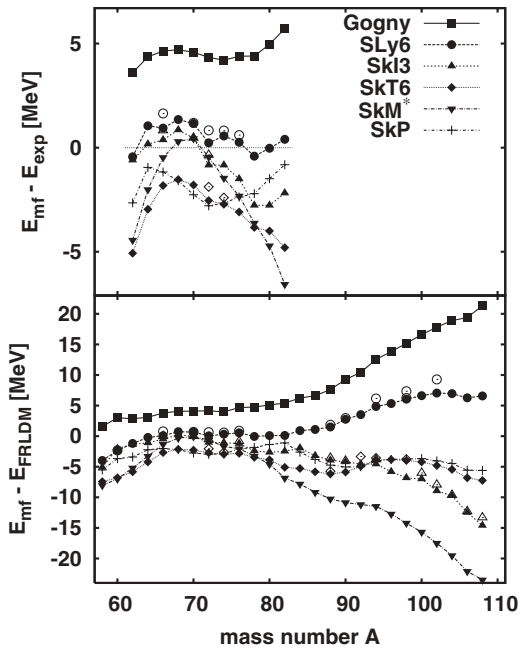

FIG. 1. Binding energies along the chain of Ge isotopes for the six forces, Gogny, SLy6, SkI3, SkT6, SkM*, and SkP, as indicated. The lower panel shows the energy differences from FRLDM values [40] and the upper panel the differences from the experimental values [41]. Filled symbols denote ground states and open symbols isomers.

The lower part of the figure shows the energies in a much broader range of isotopes drawn as the difference from FRLDM values because experimental data are not available in that deeply exotic regime. The span of the predictions grows substantially as could be expected in a regime of bold extrapolation. The trends that had already started to develop in the range of experimentally accessible nuclei (see upper panel) are basically continued with Gogny tending to lowest binding energies whereas the Skyrme forces span a broad band up to very strong binding at large neutron excess for SkM*. Simple dependencies (e.g., on the effective mass) cannot be seen. There is a mix of various influences, with symmetry energy and shell structure determined by effective mass as well as spin-orbit splitting. Note that the trend of SkI3 to stronger binding develops late on the isotopic chain (see the crossing of trends at the rather large $A = 94$). This is a consequence of the different isotopic mix in the spin-orbit term whose impact grows with neutron excess [28].

For the Skyrme energy functional there appear isomers in many cases and it is noteworthy that isomer energies are usually extremely close. This indicates that the energy landscape is very soft, often producing energetically competing shapes. The dominant shape parameter is the quadrupole deformation $Q_{2\mu} = \langle r^2 Y_{2\mu}\rangle$. For better comparison, it is useful to handle it in terms of the dimensionless quadrupole deformations

$$\beta = \sqrt{\sum_\mu \beta_{2\mu}^2}, \tag{1a}$$

$$\gamma = \text{atan}\left(\frac{\beta_{22} + \beta_{2-2}}{\sqrt{2}\beta_{20}}\right), \tag{1b}$$

$$\beta_{2\mu} = \frac{4\pi\langle r^2 Y_{2\mu}\rangle}{5\langle r^2\rangle}. \tag{1c}$$

Figure 2 is an attempt at visualizing the typical energy landscapes by showing a cut of the potential-energy surfaces (PES) along axial shapes (i.e., along β_{20}) for three examples, a proton-rich isotope ^{76}Ge, the most stable nucleus ^{82}Ge, and ^{98}Ge as a very neutron rich case. The PES are indeed very soft, particularly for ^{76}Ge and ^{82}Ge. More structures seem to develop on the proton-rich side. However, the prolate and oblate minima are softly connected along the path of triaxiality,

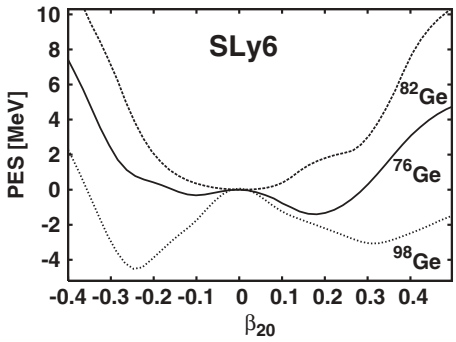

FIG. 2. Potential-energy surfaces (PES) versus axially symmetric quadrupole deformation computed with SLy6 for three selected Ge isotopes as indicated. Positive quadrupole moments correspond to prolate shapes and negative moments to oblate ones.

having, in fact, a shallow minimum at a fully triaxial shape (see Table II). The general triaxial softness of the Ge isotopes is demonstrated for the case of ^{76}Ge in Figure 3, which shows the PES in the fully triaxial deformation landscape. The weak prolate minimum extends, in fact, as a shallow valley deep into the regime of triaxiality. In this way the PES will be very soft in many cases, with the actual ground state having large shape fluctuations about the minima in the mean-field configurations. This requires, in principle, the computation of the collective ground-state correlations as done, for example, in the surveys of Refs. [42–44]. Such calculations, however, are very cumbersome and remain restricted to axial symmetry. For a first exploration, the deformations at the mean-field minima still provide useful guidelines for the structure and low-energy dynamics of the nuclei.

Figure 4 summarizes the results for deformations and pairing energies. The quadrupole deformation is quantified in terms of β and triaxiality γ as defined in Eq. (1). Table II supplies the complementary detailed numbers. All calculations agree in predicting a strong tendency to triaxial shapes for the Ge isotopes and they all, except SkP, show a clearly spherical ^{82}Ge, which is no surprise because neutron number $N = 50$

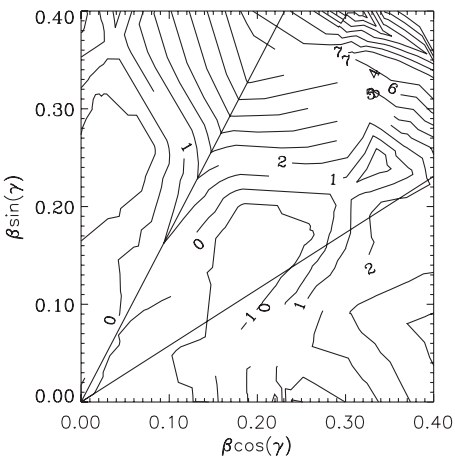

FIG. 3. Triaxial PES with SLy6 for the nucleus ^{76}Ge. The contour lines are labeled with the energy in MeV. The two straight lines indicate the directions of triaxial deformation, $\gamma = 30^\circ$ and 60°.

corresponds to a closed neutron shell. Previous theoretical works [15,16] have selected a few specific nuclei in this mass region to study nuclear exotic shapes, thus motivating the present systematic study of the isotopic chains from the proton to the neutron drip line. For example, HFB in coordinate space and the two-basis method [15] predicted the ground-state deformation of the nucleus ^{64}Ge as $\beta = 0.27$ and $\gamma = 25^\circ$, and triaxial Routhian surface calculations for ^{64}Ge yielded a well-deformed ground state at $\beta_2 = 0.3$ and $\gamma \approx 15^\circ$ [16]. They predicted similar ground-state deformations for ^{64}Ge as our Gogny, SLy6, and SkI3 calculations (as shown in Table II). At variance are the predictions of SkM*, SkP, and SkT6, which have the higher effective masses in our sample and which all yield a spherical ground state. This isotope with 32 neutrons is in the transitional region still near magic number 28 and such nuclei are sensitive to faint changes in shell structure.

At second glance, we see more interesting differences in detail. The simplest pattern is provided by the Gogny force. Except for the closed shell ^{82}Ge, all nuclei are well deformed and all of these except two are clearly triaxial. Quite similar global deformation is found also for SLy6 and SkI3. Here we have a few more spherical ground states related to the known neutron subshell closures ($N = 40$ and $N = 28$ for SLy6; $N = 40$ and $N = 70$ for SkI3). More differences are seen concerning triaxiality. Although the Gogny force predicts triaxial minima almost throughout, SLy6 and SkI3 have many axially symmetric exceptions near the stable isotopes. In these cases there are, however, many triaxial isomers and the energy separations are generally very small, which indicates that the situation is extremely soft in triaxial direction. A certain ambiguity between axial and triaxial deformations is also apparent from the zigzag pattern of triaxiality along the isotopic chain. Fully correlated calculations would smooth the fluctuations and, seen with a smoothing filter, the predictions of Gogny, SLy6, and SkI3 are in general quite similar, predicting the general importance of triaxiality for the Ge isotopes.

The situation is somewhat different for the other three Skyrme forces shown in the lower panels. These forces agree nicely with the others for the very neutron rich isotopes but yield generally smaller deformations near the valley of stability. This is related to the higher effective mass, which acts here to reduce the energy gain from deformation for the mid-shell neutron numbers. The three forces SkM*, SkP, and SkT6 have a broad transitional region of sphericity around the magic $N = 28$ before deformation develops. Further spherical dips appear at the (sub)shell closures $N = 50$ and $N = 58$. Both features are caused by shell structure (i.e., the higher effective mass of these three forces). The majority of isotopes carrying deformation are similar, although the two forces SkP and SkT6 with effective mass one have generally smaller deformations. They are also distinguished by showing broad regions of axiality around $A = 80$, where the other forces show more transitional behavior, switching between axial and triaxial shapes. In spite of all these differences in detail, we have to keep in mind that all forces agree in predicting softness and triaxiality in the region of neutron-rich Ge isotopes.

The experimental information on the ground-state shapes of the nuclei $^{70-76}$Ge [4,5] is shown for comparison. There is good agreement for Gogny, SLy6, SkI3, and SkM*. The

TABLE II. The properties of ground states (GS) and coexistent isomeric states (IS) for Ge isotopes with the Gogny HFB and Skyrme HF-BCS using the SLy6, SkI3, SkT6, SkM*, and SkP parametrizations. The eight columns represent the nucleus calculated; the force used; the type of state; the total, HF, and pairing energies; quadrupole deformation β; and triaxial deformation γ (given in degrees). The available experimental results (Exp.) are listed for comparison.

Nucleus	Force	State	E_B (MeV)	E_{HF}	E_{pair}	β	γ
^{58}Ge	Gogny	GS	−450.30	−449.94	0.36	0.24	16.6
	SLy6	GS	−455.83	−455.82	0.00	0.23	16.1
	SkI3	GS	−456.97	−456.97	0.00	0.24	17.1
	SkT6	GS	−459.30	−456.87	2.43	0.00	4.7
	SkM*	GS	−459.91	−456.42	3.49	0.00	21.4
	SkP	GS	−457.39	−453.01	4.37	0.00	4.7
^{60}Ge	Gogny	GS	−483.87	−480.60	3.27	0.17	60.0
	SLy6	GS	−489.23	−489.02	0.22	0.00	27.2
		IS	−489.21	−487.75	1.46	0.15	60.0
	SkI3	GS	−488.92	−487.71	1.21	0.20	44.0
	SkT6	GS	−493.70	−493.70	0.00	0.00	9.7
	SkM*	GS	−493.89	−493.89	0.00	0.00	43.7
	SkP	GS	−490.56	−487.75	2.80	0.00	41.9
^{62}Ge	Gogny	GS	−514.03	−511.63	2.40	0.23	23.5
	SLy6	GS	−518.07	−517.35	0.72	0.22	23.1
	SkI3	GS	−518.23	−517.29	0.94	0.24	23.1
	SkT6	GS	−522.70	−521.41	1.29	0.00	12.1
	SkM*	GS	−522.07	−520.21	1.86	0.00	12.8
	SkP	GS	−520.28	−516.34	3.94	0.00	16.0
	Exp.	GS	−517.63				
^{64}Ge	Gogny	GS	−541.52	−541.52	0.00	0.25	26.4
	SLy6	GS	−544.83	−544.83	0.00	0.24	27.6
	SkI3	GS	−545.71	−545.71	0.00	0.26	27.6
	SkT6	GS	−548.84	−548.84	0.00	0.00	24.4
	SkM*	GS	−547.89	−547.89	0.00	0.00	42.8
	SkP	GS	−546.83	−542.95	3.89	0.00	7.0
	Exp.	GS	−545.88				
^{66}Ge	Gogny	GS	−564.65	−559.63	5.02	0.24	33.8
	SLy6	GS	−568.35	−566.08	2.27	0.23	60.0
		IS	−567.65	−565.55	2.10	0.21	0.0
	SkI3	GS	−568.92	−566.57	2.34	0.24	60.0
		IS	−568.47	−566.29	2.18	0.23	0.0
	SkT6	GS	−571.11	−567.75	3.37	0.00	46.4
	SkM*	GS	−569.76	−564.89	4.87	0.00	52.9
	SkP	GS	−570.46	−563.08	7.37	0.00	57.5
	Exp.	GS	−569.29				
^{68}Ge	Gogny	GS	−586.09	−579.47	6.62	0.23	35.0
	SLy6	GS	−589.44	−584.99	4.45	0.21	39.4
	SkI3	GS	−589.94	−587.03	2.91	0.23	37.4
	SkT6	GS	−592.32	−587.62	4.70	0.12	58.3
	SkM*	GS	−590.49	−583.51	6.98	0.01	49.4
	SkP	GS	−592.38	−583.20	9.17	0.01	29.3
	Exp.	GS	−590.79				
^{70}Ge	Gogny	GS	−605.94	−598.47	7.47	0.24	32.7
	SLy6	GS	−609.36	−605.19	4.17	0.23	33.9
		IS	−609.33	−603.26	6.07	0.17	59.9
	SkI3	GS	−610.06	−606.80	3.26	0.24	36.2
		IS	−610.05	−605.78	4.27	0.15	60.0
	SkT6	GS	−612.31	−606.72	5.59	0.01	59.6
	SkM*	GS	−610.08	−602.59	7.49	0.22	29.2

TABLE II. *(Continued.)*

Nucleus	Force	State	E_B (MeV)	E_{HF}	E_{pair}	β	γ
	SkP	GS	−612.78	−603.45	9.33	0.00	22.0
	Exp.	GS	−610.52			0.23	30.9
^{72}Ge	Gogny	GS	−624.35	−616.54	7.81	0.24	30.4
	SLy6	GS	−628.45	−624.03	4.42	0.00	0.4
		IS	−627.85	−623.33	4.51	0.22	33.6
	SkI3	GS	−629.52	−623.49	6.03	0.00	0.6
		IS	−629.03	−625.30	3.73	0.20	49.9
	SkT6	GS	−631.22	−626.66	4.57	0.00	1.4
		IS	−630.56	−625.56	5.00	0.19	31.4
	SkM*	GS	−629.13	−622.41	6.72	0.24	23.6
		IS	−628.90	−619.79	9.11	0.00	5.1
	SkP	GS	−631.47	−622.98	8.49	0.00	27.9
	Exp.	GS	−628.68			0.25	33.7
^{74}Ge	Gogny	GS	−641.46	−634.46	7.00	0.24	27.5
	SLy6	GS	−645.10	−641.67	3.42	0.24	28.1
		IS	−644.84	−636.77	8.07	0.07	0.0
	SkI3	GS	−646.50	−644.18	2.32	0.23	31.2
	SkT6	GS	−648.38	−641.99	6.39	0.01	4.8
		IS	−648.06	−643.98	4.08	0.22	21.9
	SkM*	GS	−647.12	−641.11	6.01	0.24	21.9
	SkP	GS	−648.32	−638.11	10.21	0.00	4.1
	Exp.	GS	−645.66			0.28	25.9
^{76}Ge	Gogny	GS	−657.21	−651.21	6.00	0.23	24.6
	SLy6	GS	−661.34	−655.65	5.69	0.16	0.0
		IS	−661.00	−658.59	2.41	0.24	24.2
	SkI3	GS	−663.10	−658.01	5.08	0.16	0.0
		IS	−662.72	−661.91	0.81	0.26	26.1
	SkT6	GS	−664.69	−659.47	5.22	0.15	0.0
	SkM*	GS	−663.92	−658.64	5.28	0.23	20.5
	SkP	GS	−663.97	−654.45	9.51	0.13	0.0
	Exp.	GS	−661.60			0.27	28.9
^{78}Ge	Gogny	GS	−671.98	−665.14	6.84	0.18	0.0
	SLy6	GS	−676.79	−673.56	3.23	0.18	0.0
	SkI3	GS	−679.15	−676.56	2.59	0.19	0.0
	SkT6	GS	−680.21	−676.76	3.46	0.16	0.0
	SkM*	GS	−680.00	−674.06	5.94	0.17	0.0
	SkP	GS	−678.59	−671.03	7.56	0.16	0.0
	Exp.	GS	−676.38				
^{80}Ge	Gogny	GS	−685.22	−680.74	4.48	0.16	2.3
	SLy6	GS	−690.21	−687.79	2.42	0.16	0.0
	SkI3	GS	−692.95	−690.39	2.56	0.16	0.9
	SkT6	GS	−694.18	−691.73	2.45	0.14	0.0
	SkM*	GS	−694.89	−690.51	4.38	0.14	0.0
	SkP	GS	−691.67	−685.17	6.50	0.15	0.0
	Exp.	GS	−690.18				
^{82}Ge	Gogny	GS	−696.72	−689.21	7.51	0.00	12.6
	SLy6	GS	−702.03	−696.42	5.61	0.00	13.4
	SkI3	GS	−704.61	−698.48	6.12	0.01	17.3
	SkT6	GS	−707.23	−703.50	3.73	0.00	6.0
	SkM*	GS	−708.99	−704.62	4.37	0.00	15.4
	SkP	GS	−703.25	−696.44	6.81	0.11	0.9
	Exp.	GS	−702.43				
^{84}Ge	Gogny	GS	−704.51	−701.07	3.44	0.17	21.2
	SLy6	GS	−709.84	−707.16	2.68	0.16	0.4

TABLE II. *(Continued.)*

Nucleus	Force	State	E_B (MeV)	E_{HF}	E_{pair}	β	γ
	SkI3	GS	−712.69	−710.02	2.66	0.17	3.9
	SkT6	GS	−716.02	−713.06	2.96	0.12	0.8
	SkM*	GS	−718.57	−714.99	3.59	0.12	0.6
	SkP	GS	−713.36	−707.17	6.19	0.13	0.0
^{86}Ge	Gogny	GS	−711.45	−709.18	2.27	0.21	21.2
	SLy6	GS	−716.96	−716.96	0.00	0.21	21.8
	SkI3	GS	−721.26	−721.26	0.00	0.22	21.4
	SkT6	GS	−723.88	−721.66	2.22	0.13	0.0
	SkM*	GS	−727.23	−724.45	2.78	0.14	0.1
	SkP	GS	−721.87	−715.86	6.00	0.13	0.1
^{88}Ge	Gogny	GS	−716.57	−711.45	5.12	0.22	22.4
	SLy6	GS	−722.69	−720.87	1.82	0.21	0.0
		IS	−722.34	−721.55	0.79	0.22	28.2
	SkI3	GS	−728.13	−728.13	0.00	0.24	32.5
		IS	−727.75	−725.69	2.06	0.23	0.0
	SkT6	GS	−730.37	−727.59	2.79	0.08	59.9
		IS	−729.92	−728.43	1.50	0.19	0.0
	SkM*	GS	−734.45	−731.58	2.88	0.09	60.0
		IS	−734.01	−730.20	3.81	0.16	0.2
	SkP	GS	−728.92	−723.15	5.77	0.11	59.5
^{90}Ge	Gogny	GS	−720.58	−713.71	6.87	0.23	23.5
	SLy6	GS	−727.08	−726.95	0.13	0.22	22.3
		IS	−726.88	−724.91	1.97	0.22	60.0
	SkI3	GS	−734.05	−734.05	0.00	0.24	22.0
		IS	−733.88	−731.67	2.21	0.24	60.0
	SkT6	GS	−735.72	−733.03	2.68	0.00	2.8
	SkM*	GS	−740.70	−738.23	2.47	0.00	7.2
	SkP	GS	−734.88	−728.49	6.40	0.01	5.5
^{92}Ge	Gogny	GS	−723.74	−714.83	8.91	0.23	28.1
	SLy6	GS	−730.65	−728.87	1.78	0.22	33.0
	SkI3	GS	−738.72	−737.90	0.81	0.23	40.0
	SkT6	GS	−739.11	−736.64	2.47	0.16	27.0
		IS	−737.51	−733.93	3.58	0.30	0.0
	SkM*	GS	−745.35	−740.78	4.57	0.21	28.0
		IS	−744.03	−742.46	1.56	0.35	0.6
	SkP	GS	−739.17	−732.15	7.02	0.10	0.4
		IS	−739.07	−732.27	6.80	0.14	33.8
^{94}Ge	Gogny	GS	−726.31	−716.48	9.83	0.24	32.7
	SLy6	GS	−734.00	−732.18	1.82	0.24	38.5
		IS	−732.69	−729.83	2.86	0.17	0.0
	SkI3	GS	−743.40	−742.26	1.14	0.22	39.5
		IS	−742.67	−740.36	2.31	0.20	0.0
	SkT6	GS	−742.74	−740.78	1.96	0.22	34.6
		IS	−742.41	−738.90	3.51	0.14	0.1
	SkM*	GS	−750.32	−745.23	5.09	0.23	28.1
	SkP	GS	−742.94	−735.45	7.49	0.17	51.2
		IS	−742.79	−734.71	8.08	0.13	0.2
^{96}Ge	Gogny	GS	−728.29	−718.33	9.96	0.25	33.2
	SLy6	GS	−736.79	−735.64	1.15	0.24	38.1
	SkI3	GS	−747.95	−747.95	0.00	0.25	40.2
	SkT6	GS	−745.96	−743.98	1.98	0.23	33.8
	SkM*	GS	−754.86	−749.99	4.86	0.26	26.1
	SkP	GS	−745.94	−739.09	6.84	0.20	35.8

TABLE II. *(Continued.)*

Nucleus	Force	State	E_B (MeV)	E_{HF}	E_{pair}	β	γ
^{98}Ge	Gogny	GS	−729.64	−719.63	10.01	0.26	31.0
	SLy6	GS	−738.75	−737.47	1.28	0.27	31.1
		IS	−738.57	−736.13	2.44	0.21	58.8
		IS	−737.46	−733.99	3.47	0.28	1.9
	SkI3	GS	−751.62	−749.92	1.70	0.22	60.0
	SkT6	GS	−748.78	−747.12	1.66	0.26	26.9
		IS	−748.57	−746.00	2.58	0.25	0.0
	SkM*	GS	−759.01	−754.82	4.19	0.27	25.2
	SkP	GS	−748.52	−742.38	6.15	0.22	28.6
^{100}Ge	Gogny	GS	−730.39	−720.45	9.94	0.27	29.2
	SLy6	GS	−740.38	−740.38	0.00	0.30	26.6
	SkI3	GS	−754.00	−753.62	0.38	0.24	45.6
		IS	−753.03	−748.82	4.21	0.09	60.0
	SkT6	GS	−751.21	−750.26	0.94	0.28	24.6
	SkM*	GS	−762.68	−759.16	3.52	0.27	25.2
	SkP	GS	−750.68	−745.18	5.50	0.23	24.9
^{102}Ge	Gogny	GS	−730.52	−720.34	10.18	0.26	28.1
	SLy6	GS	−741.30	−741.29	0.01	0.27	31.5
		IS	−739.07	−733.34	5.73	0.00	0.1
	SkI3	GS	−757.30	−751.74	5.56	0.00	1.1
		IS	−756.30	−755.13	1.17	0.21	33.8
	SkT6	GS	−753.15	−752.52	0.63	0.25	21.3
	SkM*	GS	−765.84	−762.55	3.30	0.26	24.2
	SkP	GS	−752.39	−747.36	5.03	0.23	22.6
^{104}Ge	Gogny	GS	−730.09	−720.17	9.92	0.25	26.4
	SLy6	GS	−742.02	−741.46	0.56	0.23	23.8
	SkI3	GS	−758.71	−758.70	0.01	0.24	26.0
		IS	−758.61	−753.52	5.09	0.06	56.2
	SkT6	GS	−754.43	−753.39	1.04	0.23	22.0
	SkM*	GS	−768.51	−765.80	2.70	0.25	23.5
	SkP	GS	−753.45	−749.22	4.24	0.23	21.3
^{106}Ge	Gogny	GS	−729.10	−719.78	9.32	0.23	25.2
	SLy6	GS	−742.22	−742.11	0.11	0.24	24.8
	SkI3	GS	−760.98	−757.24	3.74	0.11	0.0
		IS	−760.79	−760.76	0.02	0.19	24.5
	SkT6	GS	−755.31	−754.93	0.38	0.23	22.0
		IS	−755.30	−752.98	2.32	0.19	7.7
	SkM*	GS	−770.60	−768.31	2.29	0.23	22.3
	SkP	GS	−754.07	−750.25	3.82	0.22	18.4
^{108}Ge	Gogny	GS	−727.47	−718.11	9.36	0.21	24.1
	SLy6	GS	−742.21	−742.21	0.00	0.19	18.9
	SkI3	GS	−763.39	−761.50	1.89	0.14	0.0
		IS	−762.10	−762.09	0.01	0.20	25.4
	SkT6	GS	−756.02	−754.91	1.11	0.18	1.0
	SkM*	GS	−772.28	−769.50	2.77	0.21	19.4
	SkP	GS	−754.39	−750.29	4.09	0.21	0.3

data seem to contradict the subshell closure at $N = 40$ seen for SLy6 and SkI3. But note that we see pronounced isomers in these cases, which indicates a great openness to triaxial effects when correlations are taken into account. Significant differences are seen for SkT6 and SkP, although also here the isomers provide a more balanced view. Note that these two forces with effective mass one produce a particularly soft PES and the pure mean-field predictions become somewhat unreliable here.

The potential energy landscape, deformation energy, and shapes are determined by an interplay of mean-field effects (shell structure) and pairing. The pairing energies are shown

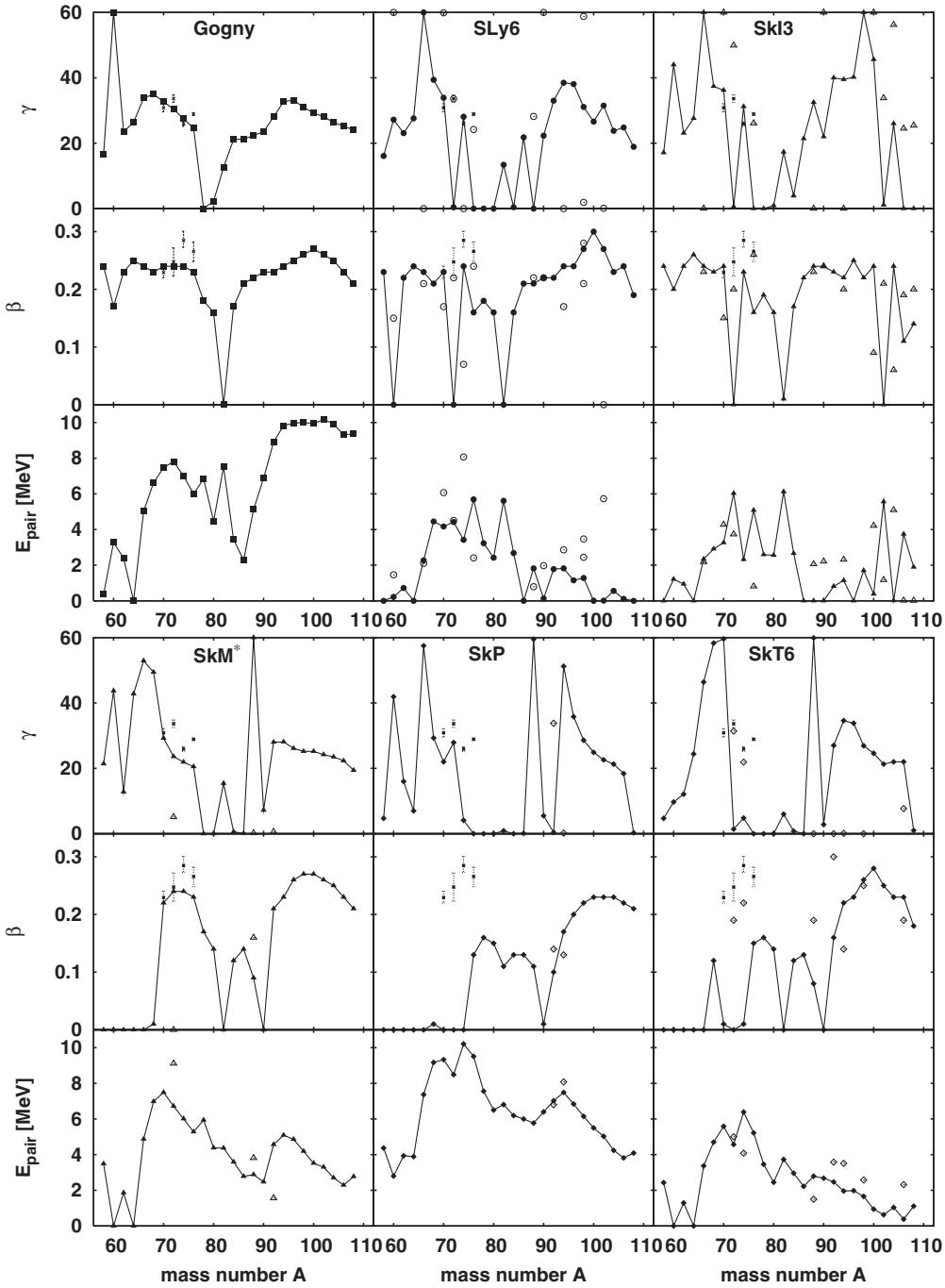

FIG. 4. The shape parameters β for total quadrupole deformation (middle panels) as well as γ for the triaxiality (upper panels) and the pairing energy (lower panels) for the six forces: Gogny (upper left panels), SLy6 (upper middle), SkI3 (upper right), SkM* (lower left), SkP (lower middle), and SkT6 (lower right). The ground-state values are shown with full symbols. Isomers are indicated by open symbols. Available experimental values for deformation and triaxiality are indicated by error bars [4,5].

as complementary information in the lower panels of Fig. 4. The Gogny force shows generally the largest pairing energies. This is due to the quite different treatment of pairing in the two models. Our Skyrme calculations use a rather sparse phase space for pairing, ± 5 MeV about the Fermi surface, whereas the Gogny calculations include a larger space. Moreover, the fitting of the pairing forces was done differently. The Skyrme forces used the full odd-even staggering as information whereas for the Gogny force, the staggering was enhanced by about 20% [20] to take into account spin polarization effects in these data [45]. But the overall scaling in pairing energy is not important because it has negligible effect on the global observables owing to a subtle balance between mean-field energy and pairing contribution. What we should compare are the trends. And even here, we see noteworthy differences. For all Skyrme forces, particularly for SLy6 and

SkI3, there is occasionally a breakdown of pairing, which indicates closeness to the phase transition because of the generally weaker pairing. A significant difference is also seen for the trends in the region of very neutron rich isotopes. The Gogny force shows a strong increase whereas all Skyrme forces tend to shrink pairing strength. This result, however, has to be considered with care. Here we are employing the pairing with a zero-range two-body force in Skyrme HFBCS, but it is known that a density-dependent pairing force enhances pairing in the regime of exotic nuclei [9,46]. The relevant information for our purposes is that the predictions on deformations, and particularly on triaxiality, are robust with respect to quite different treatments of pairing.

We have corroborated this statement by studying the effect of varying pairing strength for SLy6. We find that the overall deformation is little influenced by varying the pairing strength, especially for the nuclei in the neutron-rich region. This means that pairing does not overrule deformation effects dictated by nuclear shell structure. This statement, though, has to be taken with a grain of salt. There are sometimes exceptions near subshell closures, where a larger sensitivity to pairing is observed. Somewhat more sensitivity to pairing strength is seen for triaxiality. This is not surprising as the energy gain from triaxial deformation is smaller and can be more easily countered by pairing. The general triaxial softness, however, persists in these cases.

IV. CONCLUSION

We have systematically investigated the properties of the Ge isotopic chain from neutron number $N = 26$ to 76 in the framework of Gogny HFB and Skyrme HF plus BCS. The Gogny HFB equation, where the finite-range Gogny interaction provides both particle-hole and particle-particle correlations simultaneously, was solved in a three-dimensional harmonic oscillator basis with z-simplex and $\hat{S}_y^T$ symmetries. The coupled HF plus BCS equations, where the density-dependent Skyrme force and a δ-pairing interaction were used to treat the mean-field and pairing correlations, were solved in three-dimensional coordinate space without any symmetry restrictions. Three conclusions emerge:

(i) Both theoretical models predict that most of the Ge isotopes have triaxial features. The binding energies and the deformations β and γ agree in general very well with the available experiments. The Skyrme HF plus BCS calculations yield shape-coexistent isomers with quite different shapes but minor energy differences in many Ge isotopes. This may indicate γ-softness rather than true isomeric states, although the height of the barrier between the ground state and the isomer would yet have to be checked.

(ii) The five Skyrme parametrizations SLy6, SkI3, SkM*, SkP, and SkT6 were used for studying the effects of effective mass and spin-orbit interaction, investigating general versus specific properties in these isotopes. We found that the predictions with Gogny D1S, Skyrme SLy6, and SkI3 are quite similar with only a few exceptions. SkM* is still quite close whereas SkP and SkT6 with effective mass one predicted quite different nuclear shapes and prefer more spherical deformation for the nuclei between the proton drip line and the stable region. Comparing the properties among the Skyrme forces, we conclude that a mix of symmetry energy and shell effects determines the extrapolation to large neutron excess. From the shell effects, the effective mass is influential in all regions and the impact of the (isovector) spin-orbit interaction increases with increasing neutron number.

(iii) A variation of pairing strength with the SLy6 force has been considered to study the effect of pairing on the properties of the ground states and coexistent shape isomers. We found that the pairing strength has little effect on binding energy and quadrupole deformation. The nuclear triaxiality, however, is more sensitive to pairing strength. Triaxiality is a subtle shell effect and may be overruled by pairing.

ACKNOWLEDGMENTS

Lu Guo acknowledges support from the Alexander von Humboldt Foundation. We gratefully acknowledge support by the Frankfurt Center for Scientific Computing. The work was supported in part by the BMBF (Contract No. 06 ER 124).

[1] J. Simpson, Nucl. Phys. **A654**, 178c (1999).
[2] A. C. Mueller, Nucl. Phys. **A654**, 215c (1999).
[3] I. Tanihata, Nucl. Phys. **A654**, 235c (1999).
[4] M. Sugawara, Y. Toh, T. Czosnyka, M. Oshima, T. Hayakawa, H. Kusakari, and Y. H. *et al.*, Eur. Phys. J. A **16**, 409 (2003).
[5] Y. Toh, T. Czosnyka, M. Oshima, T. Hayakawa, H. Kusakari, M. Sugawara, Y. Hatsukawa, J. katakura, N. Shinohara, and M. Matsuda, Eur. Phys. J. A **9**, 353 (2000).
[6] M. Hasegawa, K. Kaneko, and T. Mizusaki, Phys. Rev. C **71**, 044301 (2005).
[7] K. Kaneko, M. Hasegawa, and T. Mizusaki, Phys. Rev. C **66**, 051306(R) (2002).
[8] P.-G. Reinhard, D. J. Dean, W. Nazarewicz, J. Dobaczewski, and J. A. Maruhn, Phys. Rev. C **60**, 014316 (1999).
[9] M. Bender, K. Rutz, P.-G. Reinhard, and J. A. Maruhn, Eur. Phys. J. A **8**, 59 (2000).
[10] J. P. Elliott, J. A. Evans, V. S. Lac, and G. L. Long, Nucl. Phys. **A609**, 1 (1996).
[11] E. Terán, V. E. Oberacker, and A. S. Umar, Phys. Rev. C **67**, 064314 (2003).
[12] M. V. Stoitsov, J. Dobaczewski, W. Nayarewicz, S. Pittel, and D. J. Dean, Phys. Rev. C **68**, 054312 (2003).
[13] P. Sarriguren, E. M. de Guerra, and A. Escuderos, Nucl. Phys. **A658**, 13 (1999).
[14] G. Gangopadhyay, Phys. Rev. C **59**, 2541 (1999).
[15] M. Yamagami, K. Matsuyanagi, and M. Matsuo, Nucl. Phys. **A693**, 579 (2001).
[16] P. J. Ennis *et al.*, Nucl. Phys. **A535**, 392 (1991).

[17] A. Petrovici, K. W. Schmid, F. Grümer, and A. Faessler, Nucl. Phys. **A517**, 108 (1990).
[18] M. Bender, P.-H. Heenen, and P.-G. Reinhard, Rev. Mod. Phys. **75**, 121 (2003).
[19] M. Bender, K. Rutz, P.-G. Reinhard, J. A. Maruhn, and W. Greiner, Phys. Rev. C **60**, 034304 (1999).
[20] J. Dechargé and D. Gogny, Phys. Rev. C **21**, 1568 (1980).
[21] J. L. Egido and L. M. Robledo, Phys. Rev. Lett. **70**, 2876 (1993).
[22] L. Guo, F. Sakata, and E.-G. Zhao, Nucl. Phys. **A740**, 59 (2004).
[23] P.-G. Reinhard, M. Bender, W. Nazarewicz, and T. Vertse, Phys. Rev. C **73**, 014309 (2006).
[24] J. Bartel, P. Quentin, M. Brack, C. Guet, and H.-B. Håkansson, Nucl. Phys. **A386**, 79 (1982).
[25] F. Tondeu, M. Brack, M. Farine, and J. M. Pearson, Nucl. Phys. **A420**, 297 (1984).
[26] J. Dobaczewski, H. Flocard, and J. Treiner, Nucl. Phys. **A422**, 103 (1984).
[27] E. Chabanat, E. P. Bonche, P. Haensel, J. Meyer, and R. Schaeffer, Nucl. Phys. **A635**, 231 (1998).
[28] P.-G. Reinhard and H. Flocard, Nucl. Phys. **A584**, 467 (1995).
[29] J. Friedrich and P.-G. Reinhard, Phys. Rev. C **33**, 335 (1986).
[30] F. Tondeur, Phys. Lett. **B123**, 139 (1983).
[31] S. J. Krieger, P. Bonche, H. Flocard, P. Quentin, and M. S. Weiss, Nucl. Phys. **A517**, 275 (1990).
[32] P. Fleischer, P. Klüpfel, P.-G. Reinhard, and J. A. Maruhn, Phys. Rev. C **70**, 054321 (2004).
[33] V. Blum, G. Lauritsch, J. A. Maruhn, and P.-G. Reinhard, J. Comput. Phys. **100**, 364 (1992).
[34] J. F. Berger, M. Girod, and D. Gogny, Nucl. Phys. **A428**, 23c (1984).
[35] J. F. Berger, M. Girod, and D. Gogny, Comput. Phys. Commun. **63**, 365 (1991).
[36] J. Dobaczewski, J. Dudek, S. G. Rohozinski, and T. R. Werner, Phys. Rev. C **62**, 014310 (2000).
[37] J. Dobaczewski, J. Dudek, S. G. Rohozinski, and T. R. Werner, Phys. Rev. C **62**, 014311 (2000).
[38] L. Guo, F. Sakata, and E.-G. Zhao, Phys. Rev. C **71**, 024315 (2005).
[39] L. Guo, F. Sakata, E.-G. Zhao, and J. A. Maruhn, Int. J. Mod. Phys. E **15**, 1141 (2006).
[40] P. Möller, J. R. Nix, W. D. Myers, and W. J. Swiatecki, At. Data Nucl. Data Tables **59**, 185 (1995).
[41] G. Audi, O. Bersillon, J. Blachot, and A. H. Wapstra, Nucl. Phys. **A729**, 3 (2003).
[42] P. Fleischer, P. Klüpfel, T. Cornelius, T. Bürvenich, S. Schramm, J. Maruhn, and P.-G. Reinhard, Eur. Phys. J. A **22**, 363 (2004).
[43] M. Bender, G. F. Bertsch, and P.-H. Heenen, Phys. Rev. Lett. **94**, 102503 (2005).
[44] M. Bender, G. F. Bertsch, and P.-H. Heenen, Phys. Rev. C **73**, 034322 (2006).
[45] K. Rutz, M. Bender, P.-G. Reinhard, J. A. Maruhn, and W. Greiner, Nucl. Phys. **A634**, 67 (1998).
[46] J. Dobaczewski, W. Nazarewicz, and P.-G. Reinhard, Nucl. Phys. **A693**, 361 (2001).